Journal of Solid State Chemistry **146,** 499–505 (1999)
Article ID jssc.1999.8410, available online at http://www.idealibrary.com on IDEAL®

Structural Approach and Luminescence Properties of $La_{1/6}Pb_{1/3}Zr_2(PO_4)_{17/6}(SiO_4)_{1/6}:Eu^{3+}$

K. Bakhous, F. Cherkaoui, A. Benabad, and N. El Jouhari

Laboratoire de Chimie du Solide Appliquée, Département de Chimie, Faculté des Sciences, Av. Ibn Batouta, B.P. 1014, Rabat, Morocco

and

J. M. Savariault and J. Dexpert-Ghys

Centre d'Elaboration de Matériaux et d'Etudes Structurales, CNRS, 29 rue J. Marvig, 31055 Toulouse Cedex, France

Received February 1, 1999; in revised form May 24, 1999; accepted May 25, 1999

Rare earth phosphosilicates $(Li_{1-x}Eu_x)_{1/6}Pb_{1/3}Zr_2(PO_4)_{17/6}(SiO_4)_{1/6}$ $0 \le x \le 1$ have been synthesized via a sol–gel route. The powder X-ray diffraction has been analyzed with the Nasicon-type structure. The Rietveld analysis of the structure performed in space group $R\bar{3}$ shows a statistical distribution of ions La^{3+}, Eu^{3+}, and Pb^{2+} over the positions 3*a* (occupation 10%) and 3*b* (occupation 90%) of the so-called M1 site. In agreement with these results, the Eu^{3+} luminescence analysis in these phases exhibits two sites for Eu^{3+}, both are noncentrosymmetric, revealing a local disorder in the compounds, which is also supported by the inhomogeneous broadening of the emission lines. The luminescence characteristics of this family of silicates have been investigated for various *x* values. Under excitation at 254 nm, the distinct emissions of Pb^{2+} and of Eu^{3+} are observed. The excitation of Eu^{3+} ions occurs directly via the charge transfer state or after $Pb^{2+} \rightarrow Eu^{3+}$ energy transfer. Concentration quenching of the Eu^{3+} emission is also investigated. © 1999 Academic Press

Key Words: **Nasicon; lead; lanthanum; europium; luminescence; structure.**

I. INTRODUCTION

Several oxides exhibit crystalline structures based on the $R_2(XO_4)_3$ framework made of corner-sharing RO_6 octahedra and XO_4 tetrahedra. Four structural types may be described using this unit, differing by the relative arrangement of the polyhedra, garnet (1), Nasicon (2, 3), Langbeinite (4), and $Sc_2(WO_4)_3$ (5).

The hexagonal unit cell for the Nasicon-type compounds ($Na_3Zr_2PSi_2O_{12}$) is made of units $Zr_2(PO_4/SiO_4)_3$ arranged in chains along the *c* axis; these ribbons are linked together by PO_4/SiO_4 tetrahedra in the [100] direction. Large cavities are left, one M1 site and three M2 sites by formula unit, allowing numerous insertions and/or substitutions.

Previous structural investigations of phosphates or phosphosilicates isotypic to $NaZr_2(PO_4)_3$ [NZP] (2) have shown that the rare earth element may occupy either the zirconium octahedral site (6–10) or the M1 antiprism (11, 12). Recently, a new family of phosphosilicates with the formula $Ln_{1/6}Pb_{1/3}Zr_2(PO_4)_{17/6}(SiO_4)_{1/6}$ (Ln = La, Nd, Sm, Eu, Gd, Tb, Er, and Yb) has been synthesized (13). The structural refinement by the Rietveld method in the $R\bar{3}$ group has shown that both 3*a* (000) and 3*b* (001/2) positions of the M1 site are occupied by the La^{3+} and Pb^{2+} ions.

In order to get more information on the structure of these materials, we have prepared the solid solution $(La_{1-x}Eu_x)_{1/6}Pb_{1/3}Zr_2(PO_4)_{17/6}(SiO_4)_{1/6}$ denoted $[La_{1-x}Eu_x PbZr]$ $0 \le x \le 1$. The interest in these phases resides in the optical probe properties of the Eu^{3+} ion, besides their potential applications as red emitting phosphors. The first part of this work is devoted to the structural analysis by the Rietveld method and by optical probe analysis. The second part describes the luminescent properties of the Eu^{3+} and Pb^{2+} ions in the whole composition domain $0 \le x \le 1$.

II. EXPERIMENTAL

The different compositions of the solid solution $[La_{1-x}Eu_xPbZr]$ $0 \le x \le 1$ have been prepared via a sol–gel route following the method detailed in Ref. (13). Europium oxide was chosen as the source for europium ions. The X-ray diffraction data were collected with Seifert XRD 3000TT diffractometer equipped with a graphite monochromator. The experimental conditions are gathered in Table 1. The data were then analyzed following the Rietveld method (14).

Emission and excitation optical spectra were collected with an SPEX FL212 spectrofluorimeter equipped with

0022-4596/99 $30.00

TABLE 1
Experimental Conditions and Results of the Powder Data Refinements of Phase $(La_{0.7}Eu_{0.3})_{1/6}Pb_{1/3}Zr_2(PO_4)_{17/6}(SiO_4)_{1/6}$

Diffractometer	Seifert XRD 3000
Monochromator	Graphite
Wavelength	$CuK\alpha_{1,2}$, $I(\lambda_1)/I(\lambda_2) = 0.5$
Angular domain (2θ)	10–120°
Acquisition step (2θ)	0.02°/30 s
Refinement program	Fullprof
Profile function	Pseudo-voigt
Space group	$R\bar{3}$ $Z = 6$
Hexagonal cell parameters	$a = 8.701(2)$ Å, $c = 23.410(8)$ Å
Number of reflections	1046
$R_p = \sum\lvert Y_{oi} - Y_{ci}\rvert / \sum Y_i$	0.12
$R_{wp} = [\sum w_i(Y_{oi} - Y_{ci})^2 / \sum Y_{oi}^2 w_i]^{1/2}$	0.11
$R_B = \sum\lvert I_i - I_{ci}\rvert / \sum\lvert I_i\rvert$	0.056
$R_F = \sum\lvert I_i^{1/2} - I_{ci}^{1/2}\rvert / \sum\lvert I_i\rvert^{1/2}$	0.045

a Xenon lamp. Excitation and emission wavelengths are selected by two double monochromators and the detection is ensured by a HAMAMATSU R928 photomultiplier. Emission spectra are corrected for the response curves of the monochromator and of the detector. Excitation spectra are corrected for the Xenon lamp emission curve. A nitrogen cryostat is used for the low temperature measurements.

III. STRUCTURAL APPROACH OF THE $La_{1/6}Pb_{1/3}Zr_2(PO_4)_{17/6}(SiO_4)_{1/6}:Eu^{3+}$ PHASES

Structural Analysis by X-Ray Diffraction

The powder X-ray diffraction patterns exhibit a unique [NZP]-type phase over the whole composition range of the solid solution $[La_{1-x}Eu_xPbZr]$ $0 \le x \le 1$. In Fig. 1 are plotted variations of the hexagonal unit cell parameters with x. The substitution of La^{3+} ($r_i = 1.03$ Å) for Eu^{3+} ($r_i = 0.95$ Å) (15) is accompanied by a weak increase of the a parameter, and a weak decrease of the c one.

The structure refinements were performed for the compositions $x = 0$, 0.1, 0.3, and 1 of the solid solution $[La_{1-x}Eu_xPbZr]$ with the Rietveld method starting with the atomic coordinates for the [NZP] phase (space group $R\ \bar{3}c$). The process was carried on in the $R\ \bar{3}$ space group where the atoms (*Ln*, Pb), Zr, and O are distributed over two series of independent crystallographic positions. The atomic parameters and a list of selected interatomic distances and angles found for the case $x = 0.3$ are gathered in Tables 2 and 3.

The crystallographic investigation reveals for each composition unequal occupancies of the positions 3*a* (10%) and 3*b* (90%). These positions pertain to the so-called M1 type site of the Nasicon structure and are statistically occupied by La^{3+}, Eu^{3+}, or Pb^{2+}. The M2 cavities remain empty. The oxygen polyhedron around site 3*a* appears more elongated along c (4.565(5) Å) than the one around site 3*b* (4.148(5) Å). This can be attributed to the fact that site 3*a* is less occupied than the site 3*b*, so repulsion between oxygen atoms becomes preponderant. For $x = 0.3$, the difference between Zr1–O1 and Zr1–O2, 0.17 Å, is lower than the difference between Zr2–O12 and Zr2–O22 (0.29 Å), the $Zr2O_6$ octahedra close to the 3*b* positions are then more distorted. Similar observations have been made by Alamo *et al.* in the $Ca_{0.5}Zr_2(PO_4)_3$ phase (16). These authors have shown that the Ca^{2+} cations are located in 3*b*, whereas the 3*a* position is totally empty and the ZrO_6 octahedra neighboring the occupied position are more distorted than those neighboring the vacancy. The observed distortion is still more important in the $[La_{1-x}Eu_xPbZr]$ solid solution; this effect could be assigned to the very anisotropic bonding of Pb^{2+} due to its lone pair $6s^2$. The (P, Si)O_4 tetrahedra are also very much distorted: the (P, Si)–O distances range from 1.45 to 1.65 Å and the O–(P, Si)–O angles from 106° to 117°. These lengths are within the generally accepted P–O and Si–O distance ranges (17). The (P, Si)O_4 groups appear very sensitive to their surroundings, and such distortions were already observed in compounds including lone pair elements (18) or metals in distorted coordination polyhedra (19, 20). Actually, the corner-sharing ZrO_6 and (P, Si)O_4

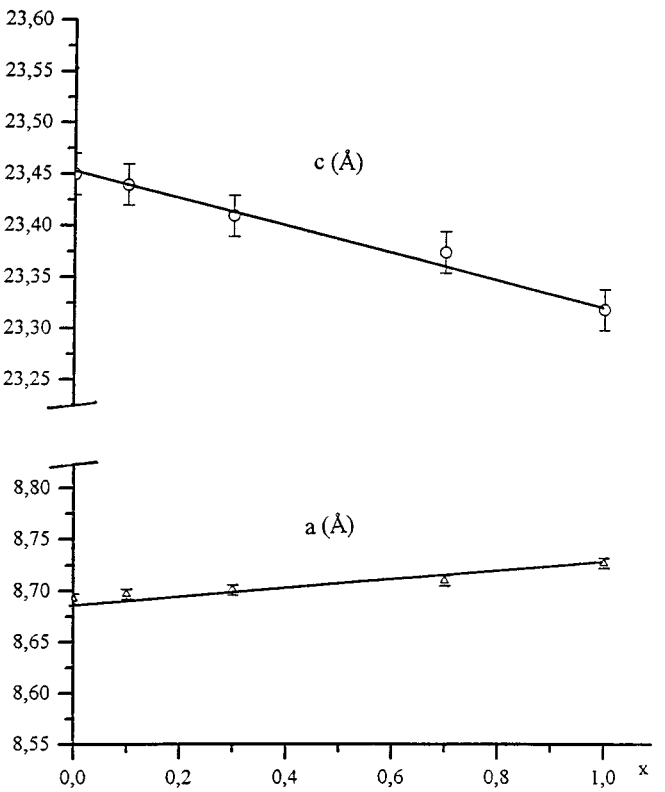

FIG. 1. Variation of the unit cell parameters a and c versus x for the solid solution $(La_{1-x}Eu_x)_{1/6}Pb_{1/3}Zr_2(PO_4)_{17/6}(SiO_4)_{1/6}$.

TABLE 2
Atomic Parameters for the Phase $(La_{0.7}Eu_{0.3})_{1/6}Pb_{1/6}Zr_2(PO_4)_{17/6}(SiO_4)_{1/6}$

Atom	Site	x	y	z	B (Å^2)
(*Ln*, Pb) 1 (10%)	3*a*	0	0	0	3.29(1)
(*Ln*, Pb) 2 (90%)	3*b*	0	0	1/2	2.93(1)
Zr1	6*c*	0	0	0.1442(1)	0.84(1)
Zr2	6*c*	0	0	0.6509(1)	0.14(1)
P, Si	18*f*	0.2857(6)	− 0.0033(9)	0.2458(3)	0.17(1)
O1	18*f*	0.149(1)	− 0.066(1)	0.2023(4)	0.90(1)
O12	18*f*	0.012(1)	− 0.183(1)	0.6941(5)	0.90(1)
O2	18*f*	0.212(1)	0.155(1)	0.0975(4)	0.90(1)
O22	18*f*	− 0.189(1)	− 0.195(1)	0.5886(4)	0.90(1)

Note. *Ln* = La, Eu.

TABLE 4
Nature and Number of $^5D_0 \rightarrow {}^7F_J$ Transitions for Eu^{3+} in C_{3i} Symmetry

J	Reps.	Nature (number) of active transitions $^5D_0 \rightarrow {}^7F_J$
0	Ag	DE (0) + DM(1)[a]
1	Ag + Eg	DM(2)
2	Ag + 2Eg	DE(0)
3	3Ag + 2Eg	DE(0) + DM(5)[a]
4	3Ag + 3Eg	DE(0)
5	3Ag + 4Eg	DE(0) + DM(7)[a]
6	5Ag + 4Eg	DE(0)

[a] See text.

polyhedra are perfectly correlated, and any distortion of the one induces distortion of the other; this kind of observation holds for the Nasicon-type materials of low symmetry (20–22).

Optical Probe Analysis

Considering the results of the crystallographic analysis, the point symmetry at each of the rare earth sites is C_{3i}. The decomposition in irreducible representations (Reps.) of the $^{2S+1}L_J$ levels with J even in this symmetry is given in Table 4. As for all the point symmetries containing an inversion center, all the intra-$4f^n$ electronic transitions of electric dipolar nature (ED) are strictly forbidden and only the magnetic dipolar (MD) transitions can be observed. In the case of Eu^{3+} (configuration $4f^6$), and considering only the emissions from the first excited level $^5D_0$, the transitions $^5D_0 \rightarrow {}^7F_{2,4,6}$ are ED and $^5D_0 \rightarrow {}^7F_1$ is MD. The determination of the nature of transitions $^5D_0 \rightarrow {}^7F_{0,3,5}$ could be made only after a complete calculations for Eu^{3+} in the considered crystal field. One may then wait for two $^5D_0 \rightarrow {}^7F_1$ lines for each of the C_{3i} sites in $[La_{1-x}Eu_xPbZr]$, and no other emission in particular in the $^5D_0 \rightarrow {}^7F_2$ region where intense lines are most commonly observed.

In Fig. 2 is plotted the Eu^{3+} emission spectrum observed for $x = 0.3$ under direct excitation of the $4f$ levels at 394 nm, with the observation made at 90 K. The line wavelengths and wavenumbers are gathered in Table 5.

The number of observed lines for the transitions $^5D_0 \rightarrow {}^7F_{0,1,2}$ is higher than that for a Eu^{3+} unique site (1, 3, 5 for $J = 0, 1, 2$), whatever its point symmetry; this means that europium ions are distributed over two different sites in the structure. The $^5D_0 \rightarrow {}^7F_0$ transition exhibits two lines denoted A (appearing at higher energy) and B; B is

TABLE 3
Selected Interatomic Distances (Å) and Angles (°) for the Phase $(La_{0.7}Eu_{0.3})_{1/6}Pb_{1/6}Zr_2(PO_4)_{17/6}(SiO_4)_{1/6}$

(*Ln*, Pb) 1	O2	2.82(1) × 6	O2–(*Ln*, Pb) 1 – O2	61.1(4) × 6
(*Ln*, Pb) 2	O22	2.66(1) × 6	O22–(*Ln*, Pb) 2 – O22	65.7(4) × 6
Zr1	O1	2.15(1) × 3	O1–Zr1–O1	84.2(7) × 3
	O2	1.98(1) × 3	O1–Zr1–O2	92.8(7) × 3
				90.2(7) × 3
			O2–Zr1–O2	92.5(7) × 3
Zr2	O12	1.93(1) × 3	O12–Zr2–O12	95.1(7) × 3
	O22	2.22(1) × 3	O12–Zr2–O22	92.4(7) × 3
				90.5(7) × 3
			O22–Zr2–O22	81.3(5) × 3
P, Si	O1	1.45(1)	O1–P–O12	107(1)
	O12	1.65(1)	O1–P–O2	117(1)
	O2	1.54(1)	O1–P–O22	107(1)
	O22	1.46(1)	O12–P–O2	107(1)
			O12–P–O22	106(1)
			O2–P–O22	112(1)

Note. *Ln* = La, Eu.

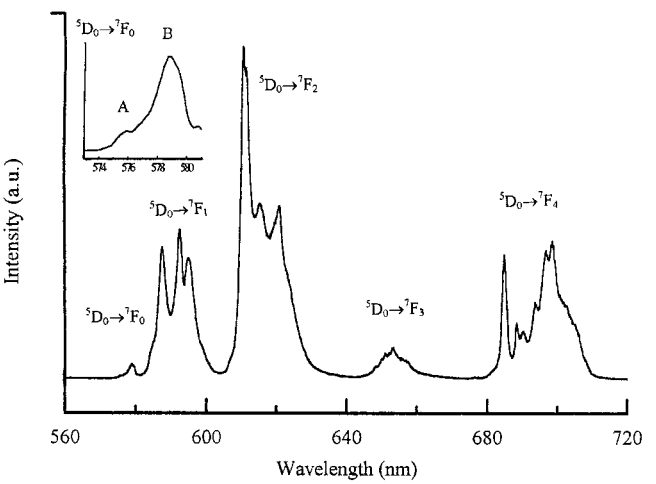

FIG. 2. Eu^{3+} emission spectrum in $(La_{0.7}Eu_{0.3})_{1/6}Pb_{1/3}Zr_2(PO_4)_{17/6}(SiO_4)_{1/6}$ ($\lambda_{exc} = 394$ nm, $T = 90$ K).

TABLE 5
Positions of the $^5D_0 \rightarrow {}^7F_J$ ($J = 0, 1, 2$) Lines Observed in $(La_{0.7}Eu_{0.3})_{1/6}Pb_{1/3}Zr_2(PO_4)_{17/6}(SiO_4)_{1/6}$ ($\lambda_{exc} = 394$ nm, $T = 90$ K)

	λ(nm)	E (cm^{-1})
$^5D_0 \rightarrow {}^7F_0$	575.7	17370
	578.9	17273
$^5D_0 \rightarrow {}^7F_1$	584.8	17098[a]
	587.5	17021
	592.5	16878
	594.9	16809
$^5D_0 \rightarrow {}^7F_2$	606.8	16479[a]
	610.9	16369
	611.7	16348
	615.3	16252
	620.8	16108
	623.1	16048[a]

[a] Shoulder.

more intense than A. Although several independent reasons my be at the origin of the observed intensity difference between A and B, for instance, a more important distortion of the site giving rise to B or energy transfer from ions in the site allocated to A toward the B site, we choose in first approximation to assign the more intense emission B to the more populated crystallographic site 3*b* (and, respectively, A to 3*a*). In the following, the whole observed emission will be considered as originating essentially from europium ions in 3*b*. In Table 6 are gathered the A and B $^5D_0 \rightarrow {}^7F_0$ transition energies and linewidths, in comparison with the equivalent data in several phosphates or silicates. The B $^5D_0 \rightarrow {}^7F_0$ energy is close to that observed in different phosphates (23–25). The data relative to the A spectrum are closer to those measured in the Nasicon-type phosphates $Eu_{1/3}Zr_2(PO_4)_3$ (12) and $Na_{1-3x}Eu_xTi_2(PO_4)_3$ (26).

The fact that one $^5D_0 \rightarrow {}^7F_0$ line is observed for each site proves that none of the two possesses an inversion center. In order to compare between different matrices the importance of the distortion of the lanthanide site with respect to an inversion center, the intensities ratio of ED over MD transitions may be considered. The value of R, ratio of the integrated emission intensities ($I_{5D0\rightarrow 7F2}/I_{5D0\rightarrow 7F1}$), is the most commonly employed for Eu^{3+}. A well documented example is that of Eu^{3+} in the cubic oxide C-Y_2O_3, in which two sites occur for rare earth, both with six oxygen first neighbors; one is C_2 and the other one C_{3i}. A rough estimation gives $R = 5$ for the C_2 site whereas for the C_{3i} site only two $^5D_0 \rightarrow {}^7F_1$ lines are observed, therefore $R = 0$ (27–30). For $(La_{0.7}Eu_{0.3})_{1/6}Pb_{1/3}Zr_2(PO_4)_{17/6}(SiO_4)_{1/6}$, R equals about 2.5. In the two related phases, $Eu_{1/3}Zr_2(PO_4)_3$ (12) and $Na_{1-3x}Eu_xTi_2(PO_4)_3$ (26), the R value is lower and may be estimated to 1.5.

All these observations point to an important lowering of the point symmetry at the rare earth site with respect to the C_{3i} one deduced from the crystallographic analysis. An analogous conclusion that is a distortion relative to the theoretical point symmetry has also been reached in Refs. (12) and (26). In the three Nasicon-type phases, Eu^{3+} lies in one (or two) M1 site, described for the first neighbors by a triangular-based antiprism of six oxygens. In $Eu_{1/3}Zr_2(PO_4)_3$, as in $Na_{1-3x}Eu_xTi_2(PO_4)_3$, only the smaller of the M1 sites is occupied, by Eu^{3+} or by Eu^{3+} and Na^+. In the $[La_{1-x}Eu_xPbZr]$ phase, both M1 sites are occupied by one of the two Ln^{3+} cations or by Pb^{2+}, yet with very different occupation levels, 90% for the more compact one ($d_{Ln\text{–}O} = 2.66$ Å) and only 10% for the less compact ($d_{Ln\text{–}O} = 2.82$ Å). The deviation with respect to the theoretical centrosymmetry is stronger for

TABLE 6
Comparison of the $^5D_0 \rightarrow {}^7F_0$ Energies and Linewidths for $(La_{0.7}Eu_{0.3})_{1/6}Pb_{1/3}Zr_2(PO_4)_{17/6}(SiO_4)_{1/6}$ and in Related Phases, versus the Europium Coordination Polyhedra

	$^5D_0 \rightarrow {}^7F_0$					
	E (cm^{-1})	$\Delta_{1/2}$	Symmetry	CN	d Eu–O	Ref.
$Eu(PO_4)$	17268	3	C_1	9	2.47	23
$KCaEu(PO_4)_2$	17301	~18	D_2	8	2.40	24
$Na_{0.2}Sr_{2.6}Eu_{0.2}(PO_4)_2$	17316	~37	C_{3v}	10	2.67	24
$La_3(SiO_4)_2Cl$:Eu	17319	~10	C_1	9	2.46	25
	17310	~10	C_{2v}	10	2.59	
$Eu_{1/3}Zr_2(PO_4)_3$	17355	~7	$(D_{3d})^a$	6	2.55	12
$Na_{1-3x}Eu_xTi_2(PO_4)_3$	17361	~48	C_{3v}	6	2.49	26
$(La_{0.7}Eu_{0.3})_{1/6}(PO_4)_{17/6}(SiO_4)_{1/6}$	17370 (A)	45	$< C_{3i}$	6	2.82	This work
	17273 (B)	68	$< C_{3i}$	6	2.66	

Note. Here, d Eu–O, indicates Eu–O distances (Å), and $\Delta_{1/2}$ indicates half height linewidth (cm^{-1}) at 80 K.
[a] See text.

$[La_{1-x}Eu_xPbZr]$ than for the two other mentioned phases; also, the $^5D_0 \rightarrow {}^7F_0$ lines are broader. There are actually in $[La_{1-x}Eu_xPbZr]$ several causes for the noncentrosymmetry at the europium site, as for the inhomogeneous broadening. The oxygen first neighbors pertain either to $(PO_4)^{3-}$ or to $(SiO_4)^{4-}$, which were not differentiated by the X-ray analysis, but very probably induce different bonding on the central ion. By the same reasoning, the second neighbors located in M1 may be Eu, La, Pb, or a vacancy, which also causes small variations in the local field experienced by the optical probe. A last origin for the distortion, and the broadening as well, is the very large M1–O distances for the 3*b* and still more for the 3*a* site, which lets us think that there is not a very well defined and thermodynamically stable position for the europium ion at the center of each antiprism.

IV. LUMINESCENT PROPERTIES OF THE PHASES $La_{1/6}Pb_{1/3}Zr_2(PO_4)_{17/6}(SiO_4)_{1/6}:Eu^{3+}$

Luminescence of the Phase $La_{1/6}Pb_{1/3}Zr_2(PO_4)_{17/6}(SiO_4)_{1/6}$

At room temperature, under UV excitation, $La_{1/6}Pb_{1/3}Zr_2(PO_4)_{17/6}(SiO_4)_{1/6}$ exhibits a light-blue luminescence, characteristic of the Pb^{2+} ion. The emission ($\lambda_{exc} = 254$ nm) and excitation ($\lambda_{em} = 410$ nm) spectra are plotted in Fig. 3. A broad emission band is observed between 300 and 600 nm with a maximum at 415 nm. The excitation is observed to start at wavelengths below 260 nm, and is still increasing at 220 nm, the limit value for a correct analysis with our experimental setup. The Stokes shift is then at least 2 eV; there is no overlap between the excitation and emission spectra, which excludes efficient energy transfer in the lead network.

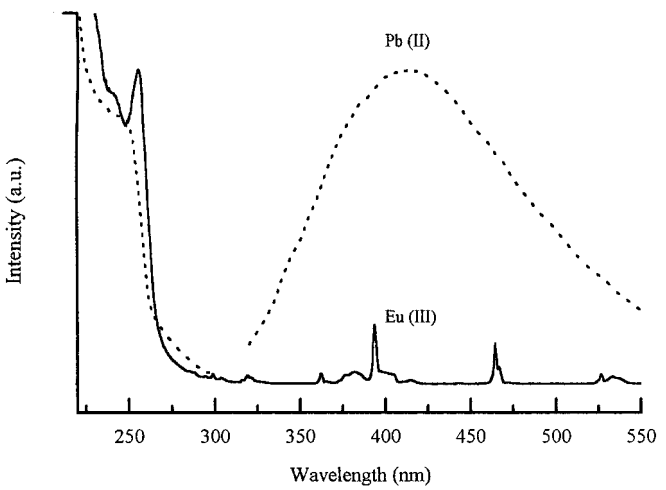

FIG. 3. Excitation ($\lambda_{em} = 410$ nm) and emission ($\lambda_{exc} = 295$ nm) spectra of Pb^{2+} in $La_{1/6}Pb_{1/3}Zr_2(PO_4)_{17/6}(SiO_4)_{1/6}$ (dotted line). Excitation spectrum of Eu^{3+} in $(La_{0.7}Eu_{0.3})_{1/6}Pb_{1/3}Zr_2(PO_4)_{17/6}(SiO_4)_{1/6}$ ($\lambda_{em} = 610.5$ nm) (solid line); $T = 300$ K.

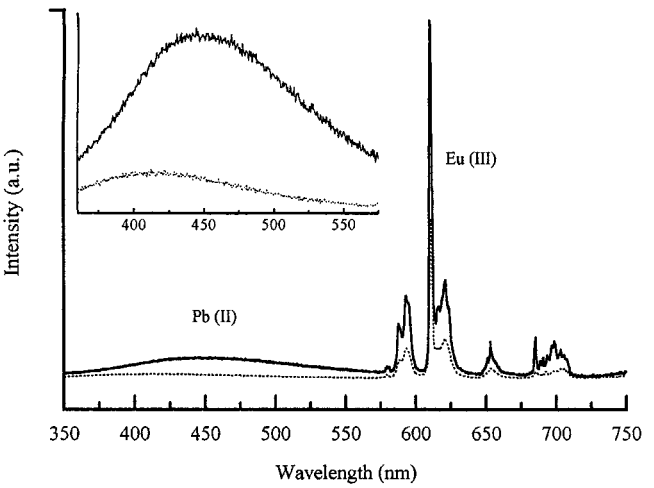

FIG. 4. Emission spectra of Pb^{2+} and Eu^{3+} in $(La_{0.7}Eu_{0.3})_{1/6}Pb_{1/3}Zr_2(PO_4)_{17/6}(SiO_4)_{1/6}$ ($\lambda_{exc} = 254$ nm, $T = 300$ K (dotted line) and 90 K (solid line)).

Luminescence of the Europium(III)-Activated Phases

In Fig. 4 are plotted the emission spectra recorded at 300 and 90 K under excitation at 254 nm of the $x = 0.3$ phase. Two distinct emissions are observed, the broad band between 300 and 600 nm characteristic of Pb^{2+} and narrow lines between 560 and 720 nm due to Eu^{3+}.

The spectrum of Pb^{2+} remains unchanged with addition of europium. Going from 90 to 300 K, the Pb^{2+} emission band shifts toward higher energies and its intensity decreases. This shift is analogous to the one observed in $SrB_6O_{10}:Pb$ (31), which has been assigned to the fact that the emission toward the fundamental level $^1S_0$ starts from the first excited level $^3P_0$ at low temperature and from the upper $^3P_1$ level at higher temperature. A quantitative analysis of the emission level lifetimes versus temperature is scheduled to investigate this hypothesis in $[La_{1-x}Eu_xPbZr]$. The Eu^{3+} $^5D_0 \rightarrow {}^7F_J$ emission lines remain unchanged at the two investigation temperatures, although the intensity decreases when T increases.

In Fig. 5 are plotted the excitation spectra monitored on the Eu^{3+} emission recorded at 90 and 300 K. The weak narrow lines correspond to the intra-$4f^6$ transitions of europium, and two intense bands are observed, pointing at 241 and 253 nm in the 90 K spectrum. At 300 K, additional intra-$4f^6$ lines appear, due to excitation from the first $^7F_1$ sublevel that is partially populated. The two bands broaden and slightly shift toward lower energies (245 and 258 nm). The 300 K Eu^{3+} excitation spectrum has been drawn in Fig. 3 in order to compare the absorption bands with those of Pb^{2+}. The 258-nm band is very distinct from the lead band and may be assigned to excitation toward the oxygen → europium (III) charge transfer state. At smaller wavelengths, the Eu^{3+} and the Pb^{2+} excitation spectra overlap. On the

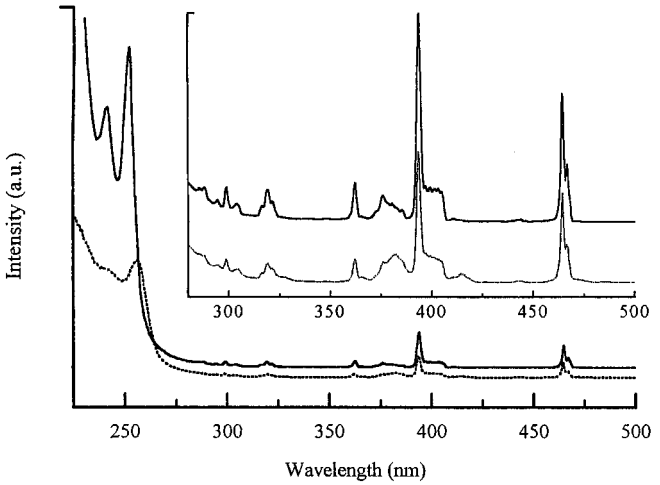

FIG. 5. Excitation spectra ($\lambda_{em} = 610.5$ nm) of Eu^{3+} in $(La_{0.7}Eu_{0.3})_{1/6}Pb_{1/3}Zr_2(PO_4)_{17/6}(SiO_4)_{1/6}$ ($T = 300$ K (dotted line) and 90 K (solid line)).

other hand, the Pb^{2+} emission band almost completely overlaps the Eu^{3+} intra-$4f^n$ excitation lines (Fig. 3). From these two last observations it is concluded that $Pb^{2+} \rightarrow Eu^{3+}$ energy transfer is highly probable. It comes out that the europium (III) emission observed under excitation at 254 nm occurs simultaneously by direct excitation in the charge transfer state and by transfer of part of the energy absorbed at the lead(II) centers. The competition for absorption at 254 nm by Pb^{2+} and Eu^{3+} and the $Pb^2 \rightarrow Eu^{3+}$ energy transfer may both play roles in the Eu^{3+} emission intensity and its variation with temperature. These processes will be systematically investigated in a next work.

The Eu^{3+} emission spectra have also been recorded for various x values in the $[La_{1-x}Eu_xPbZr]$ system. No variation in the spectra is observed, only differences in the emission intensity, integrated over the whole $^5D_0 \rightarrow {}^7F_{0-4}$ emission range. The intensities (Fig. 6) exhibit a maximum for $x = 0.2$. The decrease observed at higher europium concentrations is due to self-quenching. The emission loss with respect to the maximum value is 35% for the europium-concentrated compound $Eu_{1/6}Pb_{1/3}Zr_2(PO_4)_{17/6}(SiO_4)_{1/6}$.

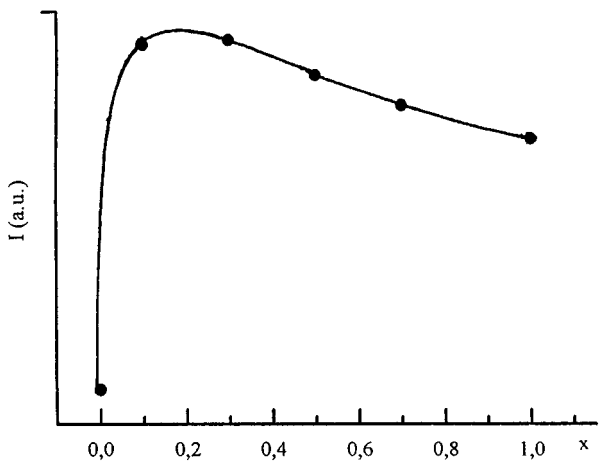

FIG. 6. Variation of the Eu^{3+} emission intensity versus x in $(La_{1-x}Eu_x)_{1/6}Pb_{1/3}Zr_2(PO_4)_{17/6}(SiO_4)_{1/6}$ ($\lambda_{exc} = 254$ nm, $T = 300$ K).

V. CONCLUSION

The structural approach of the phosphosilicates $(La_{1-x}Eu_x)_{1/6}Pb_{1/3}Zr_2(PO_4)_{17/6}(SiO_4)_{1/6}$ ($[La_{1-x}Eu_x$ PbZr]) with $0 \leq x \leq 1$ by powder X-ray diffraction and europium optical probe evidence the statistical distribution of the cations La^{3+}, Eu^{3+}, and Pb^{2+} over the two positions 3*a* (10% occupation) and 3*b* (90% occupation) denoted as the M1 cationic site. The Eu^{3+} optical probe data point to a strong deviation of the cation site from the theoretical C_{3i} point symmetry. This effect, combined with the observed broadness of the emission lines, is attributed to the various causes of local disorder in $[La_{1-x}Eu_xPbZr]$, in particular the statistical distribution of the three cations and the residual vacancies over the M1-type cationic sites and that of the two anions $(PO_4)^{3-}$ and $(SiO_4)^{4-}$ over the anionic position.

The investigation of the luminescence properties of these materials has shown the probable contribution of $Pb^{2+} \rightarrow Eu^{3+}$ energy transfers in the emission of europium (III) under excitation at the commercial wavelength (254 nm); in contrast, there is no probability for $Pb^{2+} \rightarrow Pb^{2+}$ interactions. The Eu^{3+} concentration quenching is moderate, even for the limiting composition $Eu_{1/6}Pb_{1/3}Zr_2(PO_4)_{17/6}(SiO_4)_{1/6}$.

ACKNOWLEDGMENTS

The authors would like to thank Pr. C. Parent and Dr. G. Le Flem (ICMCB, Bordeaux, France) for valuable discussions and F. Guillen (ICMCB) for the fluorescence measurements.

REFERENCES

1. H. Schwartz and L. Schmidt, *Z. Anaorg. Allg. Chem.* **387,** 31 (1972).
2. L. O. Hagman and P. Kierkegaard, *Acta Chem. Scand.* **22,** 1822 (1968).
3. H. Y.-P. Hong, *Mater. Res. Bull.* **11,** 173 (1976).
4. A. Zemann and J. Zemann, *Acta Crystallogr.* **10,** 409 (1957).
5. S. C. Abrahams and J. L. Bernstein, *J. Chem. Phys.* **45,** 2745 (1966).
6. R. Salmon, C. Parent, M. Vlasse, and G. Le Flem, *Mater. Res. Bull.* **14,** 85 (1979).
7. C. Delmas, J. C. Viala, R. Olazcuaga, G. Le Flem, P. Hagenmuller, F. Cherkaoui, and R. Brochu, *Mater. Res. Bull.* **16,** 83 (1981).
8. F. Cherkaoui, J. C. Viala, C. Delmas, and P. Hagenmuller, *Solid State Ionics* **21,** 333 (1986).
9. Y. Miyajima, Y. Saito, M. Matsuoka, and Y. Yamamoto, *Solid State Ionics* **84,** 61 (1996).
10. W. Wang and Y. Zhang, *Solid State Ionics* **86–88,** 281 (1996).

11. S. Senbhagaraman and A. M. Umarji, *J. Solid State Chem.* **85,** 169 (1990).
12. M. Alami, R. Brochu, C. Parent, L. Rabardel, and G. Le Flem, *J. Solid State Chem.* **110,** 350 (1994).
13. K. Bakhous, F. Cherkaoui, A. Benabad, and J. M. Savariault, *Mater. Res. Bull.* **34,** 263 (1999).
14. H. M. Rietveld, *Acta Crystllogr.* **20,** 508 (1966).
15. R. D. Shannon, *Acta Crystllogr. A* **23,** 751 (1976).
16. J. Alamo and J. L. Rodrigo, *Solid State Ionics* **63–65,** 678 (1993).
17. G. Bergerhoff, *in* "International Tables for Crystallography" (A. J. C. Wilson, I. U. C.), C, 683. Kluwer Academic, Dordrecht/Norwell, MA, 1992.
18. A. Mizrahi, J. P. Wignacourt, and H. Steinfink, *J. Solid State Chem.* **133,** 516 (1997).
19. W. A. Dollase, *Am. Mineral.*, **34,** 710 (1969).
20. A. Jouanneaux, A. Verbaere, Y. Piffard, A.-N. Fitch, and M. Kinoshita, *Eur. J. Solid State Inorg. Chem.* **28,** 683 (1991).
21. D. Tran Qui, J. J. Capponi, J. C. Joubert, and R. D. Shannon, *J. Solid State Chem.* **39,** 219 (1981).
22. J. P. Boilot, G. Collin, and Ph. Colomban, *Mater. Res. Bull.* **22,** 669 (1987).
23. J. Dexpert-Ghys, R. Mauricot, and M. D. Faucher, *J. Luminescence* **69,** 203 (1996).
24. C. Parent, P. Bochu, A. Daoudi, and G. Le Flem, *J. Solid State Chem.* **43,** 190 (1982).
25. B. Es-Sakhi, C. Fouassier, and A. Moudden, *Ann. Chim. Sci. Mat.* **22,** 281 (1997).
26. H. Fakrane, M. Lamire, A. El Jazouli, G. Le Flem, and R. Olazcuaga, *Ann. Chim. Sci. Mat.* **23,** 77 (1998).
27. H. Forest and G. Ban, *J. Electrochem. Soc.* **116,** 474 (1969).
28. J. Huber, K. H. Hellwege, U. Köbler, and H. Murmann, *Z. Physik* **137,** 189 (1970).
29. J. Dexpert-Ghys, Thesis, Université de Paris-Sud, 1979.
30. R. G. Pappalardo and R. B. Hunt, Jr., *J. Electrochim. Soc.* **112,** 721 (1985).
31. M. Leskela, T. Koskentalo, and G. Blasse, *J. Solid State Chem.* **59,** 272 (1985).